Large intrinsic spin Hall conductivity and anomalous Hall conductivity in monolayer $MnBi_2Te_4$

Lingpu Gong,[1] Yan Li,[1] Huaiqiang Wang,[2,*] and Haijun Zhang[1,3,†]

[1]*National Laboratory of Solid State Microstructures, School of Physics, Nanjing University, Nanjing 210093, China*

[2]*School of Physics and Technology, Nanjing Normal University, Nanjing 210023, China*

[3]*Collaborative Innovation Center of Advanced Microstructures, Nanjing University, Nanjing 210093, China*

(Received 23 August 2023; accepted 19 December 2023; published 12 January 2024)

Recently, the magnetic topological insulator $MnBi_2Te_4$ was discovered as a great platform to investigate the interplay between magnetism and topology, such as the anomalous Hall effect and the topological magnetoelectric effect. Here, we employ a first-principles approach to investigate the electronic structure of monolayer $MnBi_2Te_4$. Our calculations reveal a large spin Hall conductivity [$\sim$844.8 $(\hbar/e)$S/cm] accompanying the anomalous Hall effect due to the anticrossing bands near the Fermi level. We also surprisingly find an emergent sixfold rotational symmetry for the spin Berry curvature in the large $\boldsymbol{k}$ region of the Brillouin zone. Based on the symmetry analysis, we conclude that the spin polarization in the band structure is crucial to the emergent symmetry. Our results may provide valuable insights into understanding the large spin Hall conductivity in magnetic topological insulators.

DOI: 10.1103/PhysRevB.109.045124

I. INTRODUCTION

The spin Hall effect (SHE) is a kind of important electronic transport phenomenon in which a longitudinal charge current gives rise to a transversely polarized spin current [1–14]. This unique property provides an approach to manipulating spin without an applied magnetic field, thereby attracting great interest in the field of spintronics. Early theoretical investigations considered that the SHE emerges from the asymmetry in the spin-dependent scattering, known as the extrinsic SHE. Nonetheless, subsequent studies found the intrinsic SHE can arise solely from the electronic structure of materials, in which the spin-orbit coupling (SOC) and magnetization play an important role [15–18]. Over the past few decades, ferromagnetic (FM) materials without SOC and nonmagnetic materials with SOC have attracted much attention for generating spin currents [19–24]. Recently, researchers have shifted the focus to materials possessing both SOC and FM order, as the interplay between them leads to a wide range of spin transport behavior [25–28].

In recent years, the intrinsic magnetic topological insulator (TI) $MnBi_2Te_4$ and its related compounds were discovered as a promising platform for studying the interplay between topology and magnetism [29–46]. Experimental observations have revealed the presence of intriguing magnetic topological electronic states, such as the quantum anomalous Hall (QAH) state and the axion insulator state in $MnBi_2Te_4$ films [47–50]. In this work, we focus on the monolayer $MnBi_2Te_4$. Due to the FM order and the giant SOC, spin Hall conductivity (SHC) and net charge Hall current, known as the anomalous Hall conductivity (AHC), coexist within this system. Besides, the competition between FM order and SOC results in interesting electronic states within the system. We utilize first-principles calculations to investigate the electronic structure of monolayer $MnBi_2Te_4$ and reveal a large SHC accompanying the AHC contributed by the anticrossing bands near the Fermi level. We also find an emergent sixfold rotational symmetry in the spin Berry curvature (SBC), which can be understood by the spin polarization in the band structure.

This paper is organized as follows. The methodology for our calculations is outlined in Sec. II. In Sec. III A, we present the main results of the large SHC. In Sec. III B, we give the symmetry analysis for the band structures of monolayer $MnBi_2Te_4$ under different magnetizations. In Sec. III C, we demonstrate the emergent sixfold rotational symmetry in the SBC. Finally, we present a summary in Sec. IV.

II. METHOD

We consider a freestanding monolayer $MnBi_2Te_4$ defined as the xy plane with a vacuum layer (29 Å) in the z direction, schematically shown in Fig. 1. The first-principles calculations are carried out in the framework of the generalized gradient approximation (GGA) functional of the density functional theory through employing the Vienna *ab initio* simulation package (VASP) with projector augmented wave pseudopotentials [51–57]. The kinetic-energy cutoff of the plane wave is set to be 450 eV, and a $10 \times 10 \times 1$ k-grid mesh of the Brillouin zone (BZ) is adopted in self-consistent calculations. By considering the transition metal Mn in $MnBi_2Te_4$, the GGA+U method is adopted with U = 3 eV for Mn-d orbitals for all the calculations. In order to investigate the spin transportation, the tight-binding Hamiltonian was constructed with the maximally localized Wannier functions (MLWF) for the Mn-d, Bi-p, and Te-p orbitals through employing the Wannier90 package [58–60]. The SHC (σ_{xy}^{z}) is evaluated via

*hqwang@njnu.edu.cn
†zhanghj@nju.edu.cn

 ©2024 American Physical Society

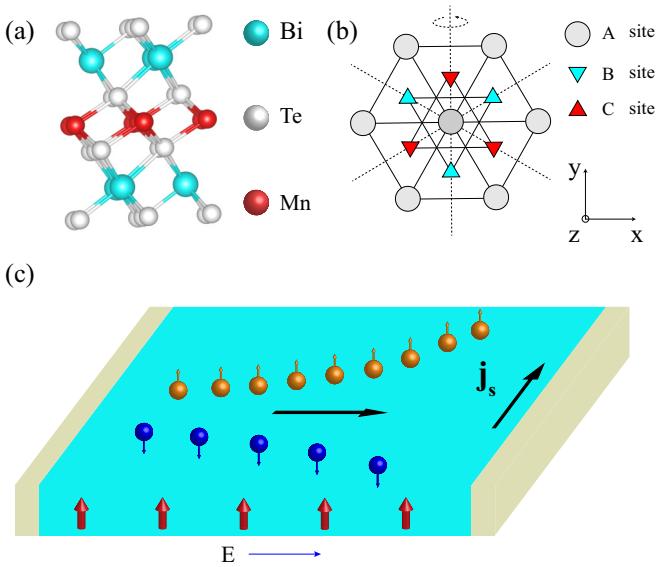

FIG. 1. (a) Lateral view of a monolayer $MnBi_2Te_4$. It has an inversion symmetry with the inversion center at the Mn site. (b) Top view of a monolayer $MnBi_2Te_4$ with three binary axes. The y axis is a binary axis for this coordinate. (c) The schematic of the transverse spin current generated by the longitudinal charge current in the monolayer $MnBi_2Te_4$ with out-of-plane ferromagnetic order.

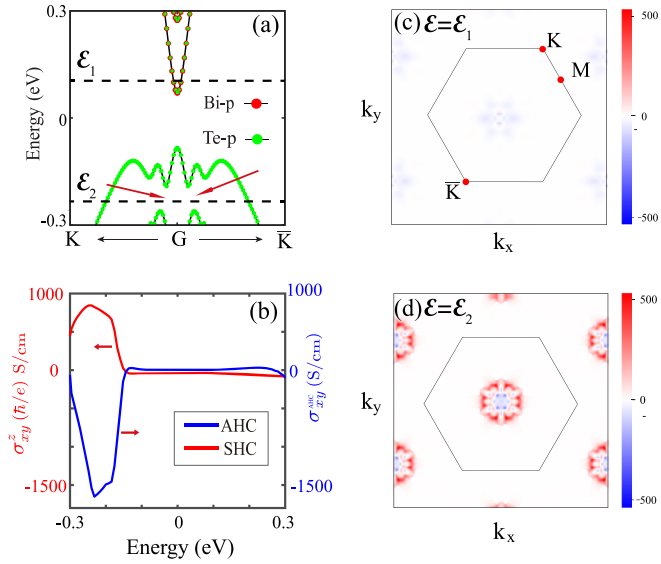

FIG. 2. (a) Fat band structure of monolayer $MnBi_2Te_4$ with projected Bi-p orbitals and Te-p orbitals. The red arrows indicate the anticrossing bands. (b) The calculated SHC and AHC versus the energy. Both SHC and AHC exhibit a prominent peak when the energy is close to the anticrossing bands. (c), (d) The k-resolved SHC when the energy level is at $\mathcal{E}_1$(c) and $\mathcal{E}_2$(d).

the Kubo formula in the linear response scheme, with the form of the summation of SBC $[\Omega^z_{n,xy}(\boldsymbol{k})]$, as follows [61]:

$$\sigma^z_{xy} = -\frac{e^2}{\hbar}\frac{1}{VN_{\boldsymbol{k}}}\sum_n\sum_{\boldsymbol{k}} f_{n\boldsymbol{k}}\Omega^z_{xy,n}(\boldsymbol{k}), \tag{1}$$

$$\Omega^z_{xy,n}(\boldsymbol{k}) = \hbar\sum_{m\neq n}\frac{-2\,\mathrm{Im}\,\langle n\boldsymbol{k}|\,\hat{j}^z_x\,|m\boldsymbol{k}\rangle\,\langle m\boldsymbol{k}|\hat{v}_y|n\boldsymbol{k}\rangle}{(\mathcal{E}_{n\boldsymbol{k}}-\mathcal{E}_{m\boldsymbol{k}})^2}, \tag{2}$$

where $f_{n\boldsymbol{k}}$ is the Fermi-Dirac distribution function, n is the band index, $\mathcal{E}_{n\boldsymbol{k}}$ is the energy eigenvalue, V is the primitive cell volume, $N_{\boldsymbol{k}}$ is the number of $\boldsymbol{k}$ points in sampling the BZ. $\hat{j}^z_i = \frac{1}{2}\{\hat{s}_z, \hat{v}_i\}$ is the spin current operator with the spin operator given by $\hat{s}_z = \frac{\hbar}{2}\hat{\sigma}_z$, and $\hat{v}_i = \frac{1}{\hbar}\frac{\partial H(\boldsymbol{k})}{\partial k_i}$ is the velocity operator. The SHC σ^z_{xy} represents that the spin current along the x direction is induced by the electric field along the y direction, where the spin current is polarized along the z direction.

III. RESULTS

A. Large spin Hall conductivity

As an MA_2Z_4 tetradymite material, $MnBi_2Te_4$ crystallizes in the rhombohedral crystal structure with the space group D^5_{3d} (No. 166) and consists of seven-atom layers (e.g., Te1-Bi1-Te2-Mn-Te3-Bi2-Te4), known as septuple layers (SLs), stacking along the z direction, seen in Fig. 1(a). It has a layered structure with a triangle lattice in the plane. The trigonal axis (threefold rotation symmetry C_{3z}) is defined as the z axis, and a bisectrix axis is defined as the y axis for the coordinate, seen in Fig. 1(b). It has the inversion symmetry with the Mn site as the inversion center.

In the ultrathin limit, monolayer $MnBi_2Te_4$ belongs to the $P\bar{3}m1$ (No. 164) space group and exhibits an FM magnetic ground state. The calculated band structure of monolayer $MnBi_2Te_4$ indicates that it has a narrow energy gap (∼0.1 eV), shown in Fig. 2(a). We can see that the conduction bands are dominated by the Bi-p orbitals, while the valence bands are dominated by the Te-p orbitals. Due to the strong finite size effect of monolayer $MnBi_2Te_4$, there is no band inversion, hence it is a topologically trivial FM insulator, unlike the bulk $MnBi_2Te_4$ [45,62,63]. However, the considerable SOC due to Bi and Te atoms is expected to facilitate a sizable SHC.

We calculate the SHC σ^z_{xy} of monolayer $MnBi_2Te_4$ versus the energy by using the Kubo formula, Eqs. (1) and (2), shown by red lines in Fig. 2(b). The valence bands exhibit an evident SHC bump with a peak value of 844.8 $(\hbar/e)$S/cm at the energy level $\mathcal{E}_2$ near anticrossing bands which is indicated by the red arrows in Fig. 2(a). It is worth noticing that the observed SHC magnitude in monolayer $MnBi_2Te_4$ is comparable to that of typical spintronic materials, such as Bi and Sb. Additionally, we calculate the k-resolved SHC at the energy level $\mathcal{E}_2$ which is the summation of SBC of the occupied bands weighted by Fermi distribution of each $\boldsymbol{k}$ point, shown in Fig. 2(d). We can see that the predominant contribution to the large SHC really comes from the anticrossing bands. The AHC against the energy is also calculated and plotted in Fig. 2(b). Conspicuously, both the AHC and SHC display a noticeable bump at the energy level $\mathcal{E}_2$, thus providing additional evidence for the same origin from the anticrossing bands. In contrast, we also notice that both the SHC and AHC at the bottom of the conduction bands are tiny. Further, we have calculated the k-resolved SHC at the energy level $\mathcal{E}_1$, as shown in Fig. 2(c), where we can see that the SHC is negligibly small. This can be attributed to the significant band splitting and the absence of anticrossing bands in the bottom of conduction bands.

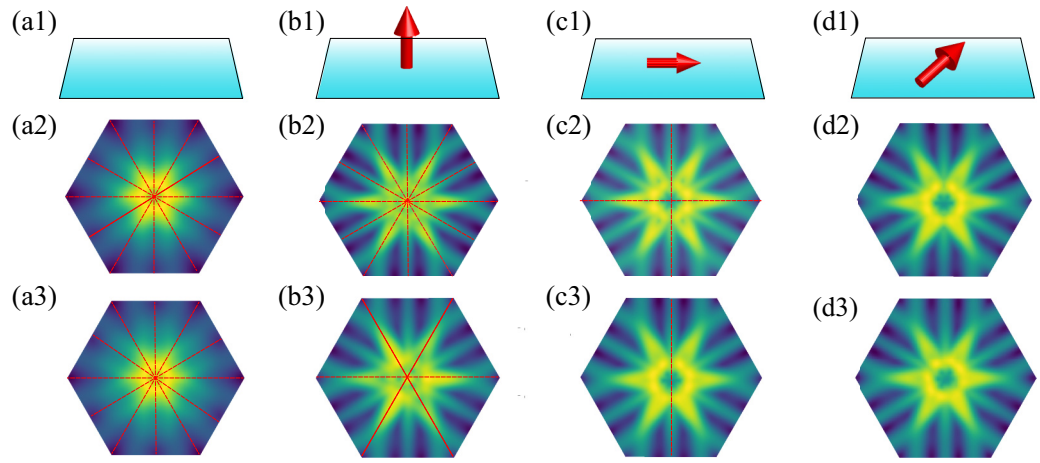

FIG. 3. (Top row) Schematics of nonmagnetic case (a1) and ferromagnetic cases with the FM moments along (b1) the z direction, (c1) the x direction, and (d1) a general low-symmetry inplane direction. The top-viewed topmost valence bands (TVBs) in the BZ under the magnetization directions corresponding to the top row in the absence (middle row) and presence (bottom row) of external electric field. The red lines denote the mirror symmetry axes.

B. Symmetry analysis of the band structure

Before the detailed analysis of the SHC, we first present the symmetry analysis of the band structure of monolayer $MnBi_2Te_4$ under different magnetizations in the presence/absence of external electric field. In the absence of magnetism, monolayer $MnBi_2Te_4$ has the mirror symmetry $\mathcal{M}_x$, the twofold rotation symmetry C_{2x}, the three-fold rotation symmetry C_{3z}, and an inversion symmetry $\mathcal{I}$ with the inversion center at the Mn site, seen in Fig. 1(b). The coexistence of C_{3z}, $\mathcal{M}_x$, and $\mathcal{T}$ symmetries leads to six mirror axes in the nonmagnetic band structure, as can be seen in Fig. 3(a2), where we take monolayer $CaBi_2Te_4$ as an example by replacing Mn atoms with nonmagnetic Ca atoms in $MnBi_2Te_4$. Moreover, when an external electric field in the z direction is introduced, the six mirror axes are well preserved due to the preservation of the above symmetries under the electric field [see Fig. 3(a3)].

Then we turn to monolayer $MnBi_2Te_4$ with the FM order along the z direction, seen in Fig. 3(b1). The FM order breaks both the mirror symmetry $\mathcal{M}_x$ and the twofold rotation symmetry C_{2x} of the lattice, but the combined $\mathcal{M}_x\mathcal{T}$ symmetry is preserved in this case. As a result, the preserved symmetries of C_{3z}, $\mathcal{I}$, and $\mathcal{M}_x\mathcal{T}$ still give rise to six mirror axes in the band structure of $MnBi_2Te_4$, seen in Fig. 3(b2). However, when an electric field is applied, the inversion symmetry is broken, and only three mirror axes are left, as shown in Fig. 3(b3). Besides, we can see the band structure satisfies $\mathcal{E}_n(k_x, k_y) = \mathcal{E}_n(k_x, -k_y)$, which is a direct result of $\mathcal{M}_x\mathcal{T}$.

Furthermore, we investigate cases where the FM order is in other directions. When it points in the x direction [see Fig. 3(c1)], the C_{3z} symmetry is obviously broken, while the $\mathcal{M}_x$ symmetry is preserved since the magnetic moment is vertical to the mirror axis. Therefore, the coexistence of the symmetries $\mathcal{I}$ and $\mathcal{M}_x$ results in two mirror axes in the band structure, shown in Fig. 3(c2). However, an external electric field will break $\mathcal{I}$, and then only one mirror axis is left along the y direction, as shown in Fig. 3(c3). At last, when the FM order is along a general in-plane direction [see Fig. 3(d1)], none of the mirror symmetries are preserved, and there is no mirror axis left both with and without an external electric field, seen in Figs. 3(d2) and 3(d3).

C. Emergent sixfold rotational symmetry

We then carry out the symmetry analysis of the SBC in this section. First, we study the nonmagnetic case by taking $CaBi_2Te_4$ as an example to plot the SBC without and with the electric field, as shown in Figs. 4(a1) and 4(a2), respectively. Under the time-reversal operation $\mathcal{T}$, we have $\mathcal{T}\hat{v}_y(\boldsymbol{k})\mathcal{T}^{-1} = -\hat{v}_y(-\boldsymbol{k})$, $\mathcal{T}\hat{j}^z_x(\boldsymbol{k})\mathcal{T}^{-1} = \hat{j}^z_x(-\boldsymbol{k})$, and $\mathcal{E}_n(\boldsymbol{k}) = \mathcal{E}_n(-\boldsymbol{k})$. With further considering the antiunitary of the $\mathcal{T}$ operator, based on the Kubo formula Eq. (2), the SBC should have $\Omega^z_{xy,n_0}(\boldsymbol{k}) = \Omega^z_{xy,n_0}(-\boldsymbol{k})$ which can be clearly seen in Fig. 4(a1). Even when an applied field is introduced, this relationship remains valid owing to the $\mathcal{T}$ symmetry, seen in Fig. 4(a2). Second, for monolayer $MnBi_2Te_4$ with out-of-plane FM ordering, the time-reversal symmetry is broken while inversion symmetry is preserved, yielding $\mathcal{E}_n(\boldsymbol{k}) = \mathcal{E}_n(-\boldsymbol{k})$. Moreover, since under the inversion operation, $\mathcal{I}\hat{j}^z_x(\boldsymbol{k})\mathcal{I}^{-1} = -\hat{j}^z_x(-\boldsymbol{k})$ and $\mathcal{I}\hat{v}_y(\boldsymbol{k})\mathcal{I}^{-1} = -\hat{v}_y(-\boldsymbol{k})$, respectively, the SBC retains the relation $\Omega^z_{xy,n0}(\boldsymbol{k}) = \Omega^z_{xy,n0}(-\boldsymbol{k})$, as shown in Fig. 4(b1). However, when an electric field is applied, the $\mathcal{I}$ symmetry is further broken and the above relation no longer holds, as shown in Fig. 4(b2). Interestingly, there is still a mirror axis left in the SBC, manifesting as $\Omega^z_{xy,n_0}(k_x, k_y) = \Omega^z_{xy,n_0}(k_x, -k_y)$, which originates from the $\mathcal{M}_x\mathcal{T}$ symmetry demonstrated in the preceding section. We can see the spin current operator velocity operator and energy dispersion transforms differently under these symmetries (see Table I), and the combination of them leads to the symmetry of SBC. It is worth noting that the SHC and AHC exhibit opposite signs [seen in Fig. 2(b)], which is determined by the orientation of the magnetic moment. Upon reversing the magnetic moment direction, the AHC changes sign while the SHC remains unchanged.

Notably, an unexpected sixfold rotational symmetry is found to emerge in the SBC of monolayer $MnBi_2Te_4$ within

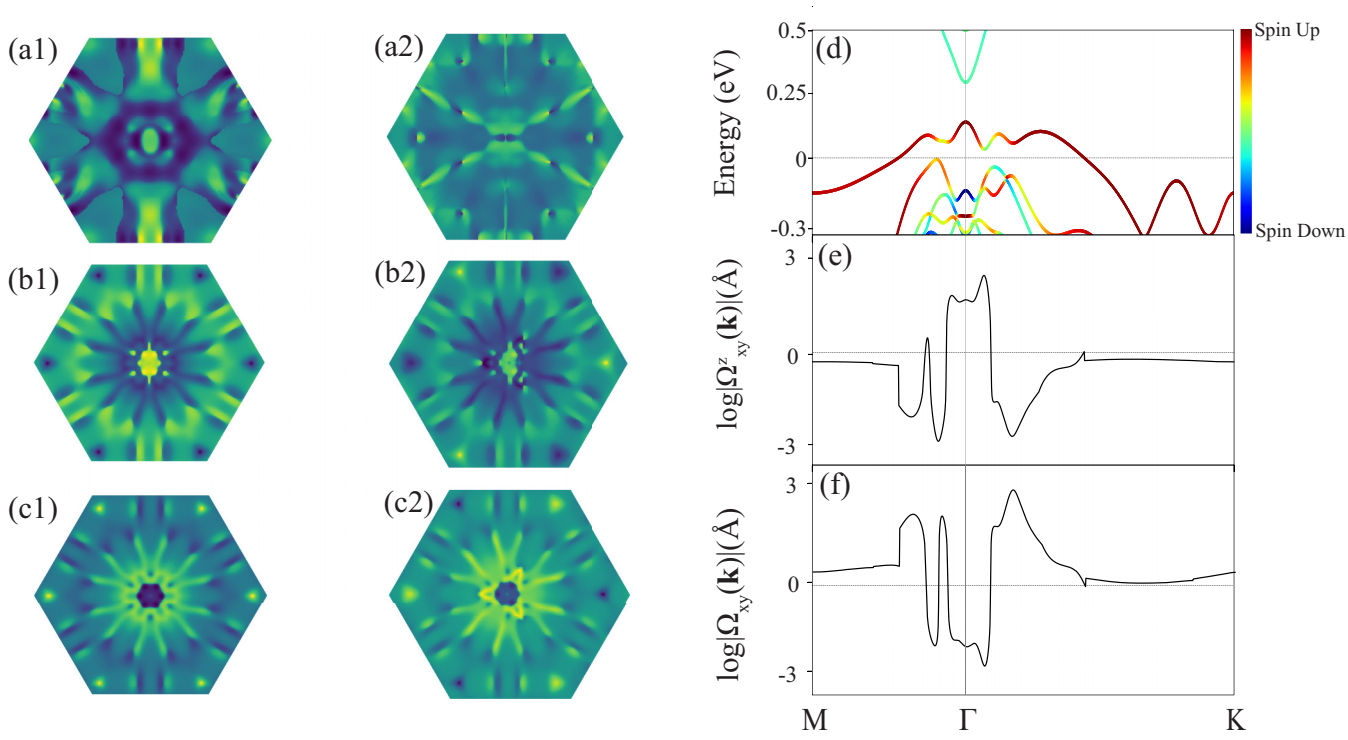

FIG. 4. The distribution of spin berry curvature (SBC) $\Omega^z_{xy,n_0}(\boldsymbol{k})$ in the absence (first column) and presence (second column) of electric field for monolayer (a1), (a2) $CaBi_2Te_4$ and (b1), (b2) $MnBi_2Te_4$. Distribution of Berry curvature $\Omega_{xy,n_0}(\boldsymbol{k})$ for $MnBi_2Te_4$ without (c1) and with (c2) electric field. (d) The band structure of monolayer $MnBi_2Te_4$ colored by the projection of the spin-z component. (e) The $\boldsymbol{k}$-resolved SHC and AHC on a log scale, respectively.

the extensive $\boldsymbol{k}$ ranges away from the Γ point, as illustrated in Figs. 4(b1) and 4(b2). This interesting property can be understood as follows. The band structure colored by the projection of the spin-z component indicates that the topmost valence band (TVB) is nearly fully spin polarized in the large $\boldsymbol{k}$ region, seen in Fig. 4(d). Therefore, it follows that $\langle n\boldsymbol{k}|\,\hat{j}^z_x\,|m\boldsymbol{k}\rangle\,\langle m\boldsymbol{k}|\,\hat{v}_y\,|n\boldsymbol{k}\rangle$ is approximately proportional to $\langle n_\uparrow\boldsymbol{k}|\,\hat{v}_{x\uparrow}\,|m_\uparrow\boldsymbol{k}\rangle\,\langle m_\uparrow\boldsymbol{k}|\,\hat{v}_{y\uparrow}\,|n_\uparrow\boldsymbol{k}\rangle$. For this reason $\Omega^z_{xy,n_0}(\boldsymbol{k})$ is proportional to the $\Omega_{xy,n_0}(\boldsymbol{k})$ near the spin-polarized TVB [seen in Figs. 4(e) and 4(f)], and they should preserve the same symmetry property. Due to the C_{3z} and the $\mathcal{I}$ symmetries of monolayer $MnBi_2Te_4$, Berry curvature $\Omega_{xy,n_0}(\boldsymbol{k})$ displays a sixfold rotational symmetry in the whole BZ. Correspondingly, in the large $\boldsymbol{k}$ region, the SBC $\Omega^z_{xy,n_0}(\boldsymbol{k})$ approximately exhibits the same feature with Berry curvature owing to the spin-polarized TVB [as shown in Figs. 4(b1) and 4(c1)]. Conversely, in the small $\boldsymbol{k}$ region, the TVB remains in a spin-mixed state due to the strong SOC, resulting in the absence of the rotational symmetry in the $\Omega^z_{xy,n_0}(\boldsymbol{k})$, which coincide with the results in previous work [64]. The contrasting nature of the two regions stems from the competition between the SOC and the FM order. When the FM order dominates the band structure, the rotational symmetry becomes evident. With further consideration of an applied electric field, due to the broken inversion symmetry, $\Omega^z_{xy,n_0}(\boldsymbol{k})$ in the large $\boldsymbol{k}$ region and thus, $\Omega_{xy,n_0}(\boldsymbol{k})$ only have the threefold rotational symmetry, as shown in Figs. 4(b2) and 4(c2).

TABLE I. The transformation property of velocity operator spin current operator and energy dispersion under three symmetries ($\mathcal{T}$, $\mathcal{I}$, $\mathcal{M}_x\mathcal{T}$).

	$\mathcal{T}$	$\mathcal{I}$	$\mathcal{M}_x\mathcal{T}$
$j^z_x(\boldsymbol{k})$	$j^z_x(-\boldsymbol{k})$	$-j^z_x(-\boldsymbol{k})$	$j^z_x(k_x,-k_y)$
$v_y(\boldsymbol{k})$	$-v_y(-\boldsymbol{k})$	$-v_y(-\boldsymbol{k})$	$-v_y(k_x,-k_y)$
$\mathcal{E}_n(\boldsymbol{k})$	$\mathcal{E}_n(-\boldsymbol{k})$	$\mathcal{E}_n(-\boldsymbol{k})$	$\mathcal{E}_n(k_x,-k_y)$

IV. SUMMARY

In summary, we focus on FM monolayer $MnBi_2Te_4$ and study its electronic structure and SHC using first-principles calculations. We find that the anticrossing bands in the TVB contribute a large SHC [∼844.8 $(\hbar/e)$S/cm] accompanying a bump in AHC, comparable to that of typical SHE materials, such as Bi and Sb. We then present the symmetry analysis for the band structure of monolayer $MnBi_2Te_4$ under different directions of the FM order, and our calculations show that the magnetism could significantly change the symmetry of the band structure. At last, we reveal an emergent sixfold rotational symmetry in the SBC, which comes from the interplay between the SOC and the FM order.

ACKNOWLEDGMENTS

This work is supported by the National Key Projects for Research and Development of China (Grant No. 2021YFA1400400), the Fundamental Research Funds for

the Central Universities (Grant No. 020414380185), the Natural Science Foundation of Jiangsu Province (Grant No. BK20200007), the Natural Science Foundation of China (Grants No. 12074181, No. 11834006, and No. 12104217), and the Fok Ying-Tong Education Foundation of China (Grant No. 161006).

[1] T. Jungwirth, J. Wunderlich, and K. Olejník, Nat. Mater. **11**, 382 (2012).
[2] M. I. Dyakonov and V. I. Perel, Phys. Lett. A **35**, 459 (1971).
[3] J. E. Hirsch, Phys. Rev. Lett. **83**, 1834 (1999).
[4] S. Zhang, Phys. Rev. Lett. **85**, 393 (2000).
[5] J. Sinova, S. O. Valenzuela, J. Wunderlich, C. H. Back, and T. Jungwirth, Rev. Mod. Phys. **87**, 1213 (2015).
[6] Y. K. Kato, R. C. Myers, A. C. Gossard, and D. D. Awschalom, Science **306**, 1910 (2004).
[7] N. F. Mott, Proc. R. Soc. A **124**, 425 (1929).
[8] N.-N. Zhao, K. Liu, and Z.-Y. Lu, Phys. Rev. B **105**, 235119 (2022).
[9] S.-B. Yu, M. Zhou, D. Zhang, and K. Chang, Phys. Rev. B **104**, 075435 (2021).
[10] J. Zhou, J. Qiao, A. Bournel, and W. Zhao, Phys. Rev. B **99**, 060408(R) (2019).
[11] A. Manchon, J. Železný, I. M. Miron, T. Jungwirth, J. Sinova, A. Thiaville, K. Garello, and P. Gambardella, Rev. Mod. Phys. **91**, 035004 (2019).
[12] E. Liu, Y. Sun, N. Kumar, L. Muechler *et al.*, Nat. Phys. **14**, 1125 (2018).
[13] Y. Sun, Y. Zhang, C. Felser, and B. Yan, Phys. Rev. Lett. **117**, 146403 (2016).
[14] Q. Yang, G. Li, K. Manna, F. Fan, C. Felser, and Y. Sun, Adv. Mater. **32**, 1908518 (2020).
[15] J. Wunderlich, B. Kaestner, J. Sinova, and T. Jungwirth, Phys. Rev. Lett. **94**, 047204 (2005).
[16] S. Murakami, N. Nagaosa, and S.-C. Zhang, Science **301**, 1348 (2003).
[17] J. Sinova, D. Culcer, Q. Niu, N. A. Sinitsyn, T. Jungwirth, and A. H. MacDonald, Phys. Rev. Lett. **92**, 126603 (2004).
[18] E. I. Rashba, Phys. Rev. B **68**, 241315(R) (2003).
[19] G. Schmidt, D. Ferrand, L. W. Molenkamp, A. T. Filip, and B. J. van Wees, Phys. Rev. B **62**, R4790 (2000).
[20] E. Saitoh, M. Ueda, H. Miyajima, and G. Tatara, Appl. Phys. Lett. **88**, 182509 (2006).
[21] T. Kimura, Y. Otani, T. Sato, S. Takahashi, and S. Maekawa, Phys. Rev. Lett. **98**, 156601 (2007).
[22] H. Zhao, E. J. Loren, H. M. van Driel, and A. L. Smirl, Phys. Rev. Lett. **96**, 246601 (2006).
[23] G. Y. Guo, S. Murakami, T.-W. Chen, and N. Nagaosa, Phys. Rev. Lett. **100**, 096401 (2008).
[24] Y. Ji, W. Zhang, H. Zhang, and W. Zhang, New J. Phys. **24**, 053027 (2022).
[25] F. Zheng, J. Dong, X. Li, M. Zhu, Y. Zhou, and J. Zhang, arXiv:2308.03111.
[26] V. P. Amin, J. Li, M. D. Stiles, and P. M. Haney, Phys. Rev. B **99**, 220405(R) (2019).
[27] G. Qu, K. Nakamura, and M. Hayashi, Phys. Rev. B **102**, 144440 (2020).
[28] T. Taniguchi, J. Grollier, and M. D. Stiles, Phys. Rev. Appl. **3**, 044001 (2015).
[29] Y. Gong, J. Guo, J. Li, K. Zhu, M. Liao *et al.*, Chin. Phys. Lett. **36**, 076801 (2019).
[30] D. Zhang, M. Shi, T. Zhu, D. Xing, H. Zhang, and J. Wang, Phys. Rev. Lett. **122**, 206401 (2019).
[31] J. Li, Y. Li, S. Du, Z. Wang, B.-L. Gu, S.-C. Zhang, K. He, W. Duan, and Y. Xu, Sci. Adv. **5**, eaaw5685 (2019).
[32] M. M. Otrokov, I. I. Klimovskikh, H. Bentmann, D. Estyunin, A. Zeugner, Z. S. Aliev *et al.*, Nature (London) **576**, 416 (2019).
[33] K. He, npj Quantum Mater. **5**, 90 (2020).
[34] Y.J. Chen, L.X. Xu, J.H. Li, Y.W. Li, H.Y. Wang, C.F. Zhang, H. Li, Y. Wu, A.J. Liang, C. Chen, S.W. Jung, C. Cacho, Y.H. Mao, S. Liu, M.X. Wang, Y.F. Guo, Y. Xu, Z.K. Liu, L.X. Yang, Y.L. Chen, Phys. Rev. X **9**, 041040 (2019).
[35] Y.-J. Hao, P. Liu, Y. Feng, X.-M. Ma, E.F. Schwier, M. Arita, S. Kumar, C. Hu, R. Lu, M. Zeng, Y. Wang, Z. Hao, H.-Y. Sun, K. Zhang, J. Mei, N. Ni, L. Wu, K. Shimada, C. Chen, Q. Liu, C. Liu, Phys. Rev. X **9**, 041038 (2019).
[36] H. Li, S.Y. Gao, S.F. Duan, Y.F. Xu, K.J. Zhu, S.J. Tian, J.C. Gao, W.H. Fan, Z.C. Rao, J.R. Huang, J.J. Li, D.Y. Yan, Z.T. Liu, W.L. Liu, Y.B. Huang, Y.L. Li, Y. Liu, G.B. Zhang, P. Zhang, T. Kondo, S. Shin, H.C. Lei, Y.G. Shi, W.T. Zhang, H.M. Weng, T. Qian, H. Ding, Phys. Rev. X **9**, 041039 (2019).
[37] B. Chen, F. Fei, D. Zhang, B. Zhang, W. Liu, S. Zhang, P. Wang, B. Wei, Y. Zhang, Z. Zuo *et al.*, Nat. Commun. **10**, 4469 (2019).
[38] E. D. L. Rienks, S. Wimmer, J. Sánchez-Barriga, O. Caha, P. S. Mandal, J. Růžička *et al.*, Nature (London) **576**, 423 (2019).
[39] R.C. Vidal, A. Zeugner, J.I. Facio, R. Ray, M.H. Haghighi, A.U.B. Wolter, L.T. CorredorBohorquez, F. Caglieris, S. Moser, T. Figgemeier, T.R.F. Peixoto, H.B. Vasili, M. Valvidares, S. Jung, C. Cacho, A. Alfonsov, K. Mehlawat, V. Kataev, C. Hess, M. Richter, B. Buchner, J. vandenBrink, M. Ruck, F. Reinert, H. Bentmann, A. Isaeva, Phys. Rev. X **9**, 041065 (2019).
[40] I. I. Klimovskikh, M. M. Otrokov, D. Estyunin, S. V. Eremeev *et al.*, npj Quantum Mater. **5**, 54 (2020).
[41] T. Zhu, H. Wang, H. Zhang, and D. Xing, npj Comput. Mater. **7**, 121 (2021).
[42] H. Wang, D. Wang, Z. Yang, M. Shi, J. Ruan, D. Xing, J. Wang, and H. Zhang, Phys. Rev. B **101**, 081109(R) (2020).
[43] D. Wang, H. Wang, D. Xing, and H. Zhang, Sci. China: Phys., Mech. Astron. **66**, 297211 (2023).
[44] T. Zhu, H. Wang, D. Xing, and H. Zhang, Phys. Rev. B **106**, 075103 (2022).
[45] Y. Li, Z. Jiang, J. Li, S. Xu, and W. Duan, Phys. Rev. B **100**, 134438 (2019).
[46] J. Zhang, D. Wang, M. Shi, T. Zhu, H. Zhang, and J. Wang, Chin. Phys. Lett. **37**, 077304 (2020).
[47] Y. Deng, Y. Yu, M. Z. Shi, Z. Guo, Z. Xu, J. Wang, X. H. Chen, and Y. Zhang, Science **367**, 895 (2020).
[48] C. Liu, Y. Wang, H. Li, Y. Wu, Y. Li *et al.*, Nat. Mater. **19**, 522 (2020).
[49] J. Cai, D. Ovchinnikov, Z. Fei, M. He, T. Song *et al.*, Nat. Commun. **13**, 1668 (2022).

[50] D. Ovchinnikov, X. Huang, Z. Lin, Z. Fei, J. Cai, T. Song, M. He, Q. Jiang, C. Wang, H. Li *et al.*, Nano Lett. **21**, 2544 (2021).
[51] G. Kresse and J. Furthmüller, Phys. Rev. B **54**, 11169 (1996).
[52] G. Kresse and J. Hafner, Phys. Rev. B **49**, 14251 (1994).
[53] P. Hohenberg and W. Kohn, Phys. Rev. **136**, B864 (1964).
[54] W. Kohn and L. J. Sham, Phys. Rev. **140**, A1133 (1965).
[55] J. P. Perdew, K. Burke, and M. Ernzerhof, Phys. Rev. Lett. **77**, 3865 (1996).
[56] S. L. Dudarev, G. A. Botton, S. Y. Savrasov, C. J. Humphreys, and A. P. Sutton, Phys. Rev. B **57**, 1505 (1998).
[57] P. E. Blöchl, Phys. Rev. B **50**, 17953 (1994).
[58] N. Marzari and D. Vanderbilt, Phys. Rev. B **56**, 12847 (1997).
[59] I. Souza, N. Marzari, and D. Vanderbilt, Phys. Rev. B **65**, 035109 (2001).
[60] G. Pizzi, V. Vitale, R. Arita, S. Blügel, F. Freimuth, G. Géranton, M. Gibertini, D. Gresch *et al.*, J. Phys.: Condens. Matter **32**, 165902 (2020).
[61] J. Qiao, J. Zhou, Z. Yuan, and W. Zhao, Phys. Rev. B **98**, 214402 (2018).
[62] J.-Q. Yan, Q. Zhang, T. Heitmann, Z. Huang, K. Y. Chen, J.-G. Cheng, W. Wu, D. Vaknin, B. C. Sales, and R. J. McQueeney, Phys. Rev. Mater. **3**, 064202 (2019).
[63] B. Li, J.-Q. Yan, D. M. Pajerowski, E. Gordon, A.-M. Nedić, Y. Sizyuk, L. Ke, P. P. Orth, D. Vaknin, and R. J. McQueeney, Phys. Rev. Lett. **124**, 167204 (2020).
[64] K. Yang, Y. Wang, and C.-X. Liu, Phys. Rev. Lett. **128**, 166601 (2022).